AGU PUBLICATIONS

Geophysical Research Letters

RESEARCH LETTER
10.1002/2017GL073305

Key Points:
- The Galileo Probe observed a layer of air likely adjusted by slantwise convection from 1 to 3 bars
- The observed Galileo static stability in the 1-3 bar layer is misleading and actually neutral
- A full scale height is therefore neutral to dry convection in the "hot spot" location of the Galileo Probe

Correspondence to:
M. E O'Neill,
morgan.e.oneill@gmail.com

Citation:
O'Neill, M. E, Y. Kaspi, and L. N. Fletcher (2017), Galileo probe interpretation indicating a neutrally stable layer in the Jovian troposphere, *Geophys. Res. Lett.*, *44*, 4008–4017, doi:10.1002/2017GL073305.

Received 1 MAR 2017
Accepted 22 APR 2017
Accepted article online 26 APR 2017
Published online 14 MAY 2017

Galileo probe interpretation indicating a neutrally stable layer in the Jovian troposphere

Morgan E O'Neill[1], Yohai Kaspi[1], and Leigh N. Fletcher[2]

[1]Department of Earth and Planetary Sciences, Weizmann Institute of Science, Rehovot, Israel, [2]Department of Physics and Astronomy, University of Leicester, Leicester, UK

Abstract The sole in situ measurement of a giant planet atmosphere comes from the Galileo probe, which plunged through Jupiter's weather layer at 6.5°N and measured a remarkably stable atmospheric temperature profile. Horizontal winds were observed to substantially increase from 1 to 3 bars, in a region of relatively low static stability. We show that this high-shear region indicates the best possibility of zero potential vorticity and resulting slantwise convection and suggest that the fluid here could potentially be adiabatic. We generalize an expression to determine lapse rates along constant angular momentum surfaces for deep atmospheres at any latitude.

1. Introduction

The gas giant planets have significant internal heat left over from their early formation, resulting in a likely well-mixed (adiabatic), convecting interior [e.g., *Guillot et al.*, 2004]. This heat, in addition to sunlight, ultimately drives the jets and storms observed in the upper weather layer (troposphere) [*Ingersoll*, 1990]. The upper troposphere is expected to be slightly stable because of low opacity, solar insolation, and moist convection, and the exact stability affects the planets' visible cloud layers and how efficiently they can cool to space. Characterizing this stability is a major challenge for planetary science because it helps constrain the thermal evolution of the solar system's oldest planets [*Hubbard*, 1977].

To date, there exists only a single in situ vertical profile, or sounding, of a giant planet weather layer. The Galileo probe (GP) entered the Jovian atmosphere at 6.5°N and reported temperature, wind, and chemical data from the stratosphere down to a pressure of 22 bars, deep in the troposphere [*Young*, 1998]. The probe reported a surprisingly stable, relatively cloud-free atmosphere [*Seiff et al.*, 1998; *Magalhães et al.*, 2002, hereinafter MSY], with an initial strong increase in horizontal winds from 1 to 3 bars, before leveling out to a nearly constant horizontal wind profile [*Atkinson et al.*, 1997]. These characteristics are often sensibly attributed to the highly anomalous environment encountered by the GP [*Orton et al.*, 1998; *Showman and Dowling*, 2000] (referred to as a "hot spot" because local low opacity permits sounding of the deeper, warmer layers), which is widely considered to be not representative of global dynamics.

The measured static stability varied significantly with depth, from +0.5 K km^{-1} to negative, gravitationally unstable layers. The focus of this paper is the high-shear region from 1 to 3 bars, where static stability was relatively low (0.04 K km^{-1}) but positive. The nondimensional Richardson number $Ri = N^2/(\partial u/\partial z)^2$ is a ratio between static stability and vertical wind shear, for squared Brunt-Väisälä frequency $N^2 = (g/\theta_0)\partial\theta/\partial z$, local gravitational acceleration g, and a reference dry potential temperature θ_0. MSY remark that the inverse correlation between static stability and vertical shear magnitude in the high-shear region was unexpected and leads to an Ri of approximately 0.25, putatively attributed to local gradient wind balance [*Showman and Ingersoll*, 1998]. *Flasar and Gierasch* [1986] proposed that Jupiter's observed mesoscale waves propagate in a layer below 670 mbar where $Ri > 0.25$, but upon reaching 670 mbar, the waves evanesce through a wave trapping region where $Ri < 0.25$. They hypothesized that, outside the wave trapping region, Ri must be near 1 to maintain the coherence of the single observed wave mode (corroborated independently by *Allison et al.* [1995]). MSY note that the *Flasar and Gierasch* [1986] model is qualitatively similar to the upper tropospheric GP observations, where the high-shear region may function as the proposed wave trapping region.

MSY and others who seek to explain the dynamics responsible for the GP sounding have neglected the possible role of symmetric instability (SI), which generally has the fastest growth rate for flows of $Ri < 1$. In this

paper we suggest that SI was likely observed by the GP in the high-shear region, which has important implications for evaluation of the static stability in that layer. Section 2 reviews SI literature, with emphasis on the applicability of SI to the turbulent 3-D atmospheres of the giant planets. Section 3 discusses the aspects of previous GP analysis relevant to SI, describes the observations used, and demonstrates that potential vorticity in the high-shear region is possibly 0. Section 4 presents a generalized method for assessing observed lapse rates in $Ri = 1$ regions against the adiabatic hypothesis and shows results for a modified lapse rate in the high-shear region. Section 5 explores the possibility of observing slantwise convection from Earth and space, and section 6 concludes with a discussion.

2. Symmetric Instability in a 3-D Fluid

A three-dimensional, stably stratified, rotating fluid can manifest a range of different instabilities. These instabilities may occur in series or in parallel, and they modify the mean state of the atmosphere. SI is a 2-D generalization of gravitational and inertial instability, additionally generalizing for nonparallel gravitational and spin axes. SI occurs when a fluid has potential vorticity (PV$\propto \nabla\theta \times \nabla M$ for potential temperature θ and absolute angular momentum M) of the opposite sign of the local Coriolis parameter (i.e., negative in the Northern Hemisphere) [*Hoskins*, 1974], and the instability readjusts the fluid back to PV = 0.

The Richardson number can help indicate whether baroclinic instability, SI, or Kelvin-Helmholtz instability has the fastest growth rate for a given fluid [*Stone*, 1966]. For a shallow flow that varies only in the vertical, as in the Eady model [*Eady*, 1949], the critical $Ri_c = 1$ indicates that PV is 0 [*Stone*, 1966; *Charney*, 1973]. This is of particular interest at low latitudes on a fluid planet as large and rapidly rotating as Jupiter, for which the global bulk Richardson number may be near unity (1.2–4 [*Allison et al.*, 1995]). The addition of horizontal shear sets $Ri_c = 2\Omega \sin\phi/(2\Omega \sin\phi - \partial u/\partial y)$ [*Hoskins*, 1974], for latitude ϕ. The horizontal component of the Coriolis force is appropriate to retain for the giant planets and further complicates the critical Richardson number. The stability phase space for deep, sheared flow was explored by *Itano and Maruyama* [2009], *Jeffery and Wingate* [2009], and *deVerdiere* [2012]. They showed that the presence of SI becomes a function of not just *Ri* but also Rossby numbers $Ro_z = (-\partial u/\partial y)/(2\Omega \sin\phi)$ and $Ro_y = (\partial u/\partial z)/(2\Omega \cos\phi)$ (following notation of *deVerdiere* [2012]). A stability asymmetry due to Ro_z occurs, and near-equatorial flows with cyclonic horizontal shear are stabilized for a broader range of *Ri* and Ro_y than those with anticyclonic horizontal shear. In all cases, PV < 0 is necessary and sufficient to excite SI in an inviscid 2-D flow [*Ooyama*, 1966].

Most of the literature that has explored the conditions leading to SI concerns strictly 2-D flows [e.g., *Stone*, 1966, 1967; *Emanuel*, 1983b; *Thorpe and Rotunno*, 1989; *Straneo et al.*, 2002; *Fantini and Malguzzi*, 2008; *Taylor and Ferrari*, 2009; *deVerdiere*, 2012; *O'Neill and Kaspi*, 2016] or linearized flows [e.g., *Stone*, 1970; *Jeffery and Wingate*, 2009]. In a fully 3-D, turbulent fluid such as Jupiter, the relevance of SI is less clear because it is formally a 2-D phenomenon, and determining the fastest and most influential instability for a particular parameter space is of considerable difficulty. *Dunkerton* [1983] examined equatorial "nonsymmetric instability" in which nonzero zonal wavenumber instabilities grow and are arrested by viscosity. *Stone* [1966, 1970] showed that rotated modes (rotated horizontally relative to the direction of wind shear) are unstable, though not as unstable as the symmetric modes. These modes are a mixed baroclinic symmetric instability [*Arobone and Sarkar*, 2015] (pure baroclinic and symmetric modes are orthogonal), with growth rates that can rival those of the pure modes [*Stamper and Taylor*, 2017]. *Jones and Thorpe* [1992] were the first to study nonlinear development in a fully 3-D model and showed that rotated modes are more likely to occur than purely symmetric modes. Energy for the growing mixed instability is thus drawn from both the baroclinic reservoir (available potential energy) and the shear flow (kinetic energy).

A limited number of numerical studies have examined the fully turbulent evolution of a flow with SI [*Jones and Thorpe*, 1992; *Taylor and Ferrari*, 2009; *Arobone and Sarkar*, 2015; *Stamper and Taylor*, 2017], finding that horizontally elongated but finite frontal regions exhibit robust SI signatures and corresponding vertical tilted features. These more recent numerical studies support the decades old interpretation of banded midlatitude convection on Earth [*Bennetts and Hoskins*, 1979; *Emanuel*, 1983a, 1983b; *Sanders*, 1986]. SI can manifest in fully turbulent atmospheres and ocean mixed layers, and its 2-D nature need only be satisfied on an order-of-magnitude basis [see *Thomas et al.*, 2016, Appendix A]. Observational campaigns have observed negative or zero PV under specific frontal conditions in both the terrestrial atmosphere [e.g., *Emanuel*, 1979] and ocean [*D'Asaro et al.*, 2011; *Thomas et al.*, 2013, 2016].

How does a fluid with negative PV respond to the instability? Whereas a gravitationally unstable fluid can rearrange itself in order to remove the instability, a negative PV fluid cannot be adiabatically rearranged to increase the materially conserved PV. Instead, PV is ultimately modified by boundary fluxes or mixing with nearby reservoirs of higher PV [*Thorpe and Rotunno*, 1989]. Higher-PV air dilutes the negative PV via mixing, driving *Ri* back to unity and neutralizing the instability [*Stone*, 1966]. The mixing is accelerated by Kelvin-Helmholtz instabilities [*Taylor and Ferrari*, 2009; *Stamper and Taylor*, 2017]. Upon $Ri = 1$, SI is no longer the dominant growing mode, and baroclinic instability takes over [*Haine and Marshall*, 1998].

3. Symmetric Instability in the Galileo Probe Observations

The GP observed a significant increase in horizontal wind with depth, from about 110 m s^{-1} at 1 bar to 170 m s^{-1} at 3 bars. MSY used linear gravity wave theory to explore where *Ri* can be expected to cross the convection threshold of 0.25. They suggest that $Ri = 0.25$ in the region $1.25 < p < 3$ bars and $9 < p < 15$ bars, the former of which is coincident with the high-shear region. These low *Ri* layers are considered "convective" in contrast with the "dynamically stable" regions where $Ri > 0.25$, in which inertia gravity waves can propagate, yet the lapse rates still suggest static stability.

MSY's discussion of the critical $Ri = 0.25$ lacks mention of the regime important to symmetric instability, which dominates for $0.25 < Ri < 1$. In such a regime, fluid mixes in nearly horizontal alternating sheets and lapse rates are properly assessed along correspondingly horizontal angular momentum surfaces. Positive dry static stability measured strictly in the vertical direction can incorrectly imply a stratified fluid, when in such circumstances the fluid is likely adiabatic and thus neutral to dry convection [*Emanuel*, 1983a, 1983b, 1985].

Recall that the low latitude of entry makes the GP trajectory nearly orthogonal to the spin axis. An adiabatic, inertially stable fluid exhibits increasing angular momentum from the spin axis. A remarkable and largely overlooked aspect of the high-shear region is that *M*, which has contributions from both the planetary rotation and the local zonal flow, *increases* with depth significantly (Figure 1), because the horizontal winds increase so rapidly with depth. In the case of the high-shear region, the angular momentum gradient is directed toward the spin axis because the observed negative wind shear is an order of magnitude larger than the outward pointing planetary component $2\Omega \sin \phi$. The addition of a sufficiently large stable stratification also orthogonal to the spin axis can stabilize an otherwise inertially unstable flow.

To calculate the relative orientations of ∇M and $\nabla \theta$, wind, pressure, gravity, and altitude data were taken from NASA's Galileo Probe Doppler Wind Experiment and the Atmospheric Structure Instrument. The observed lapse rate Γ_z was digitally extracted from Figure 7 of MSY. The MSY lapse rate is highly volatile with depth, including regions of large static instability (where the authors note that the instruments were well outside their calibrated range) and large positive static stability. The lapse rate is expressed as a dry potential temperature θ, where $\theta = T(p_0/p)^{(R_{H_2}/c_p)}$ for observed temperature *T*, reference pressure p_0, and a ratio of specific heats $R_{H_2}/c_p \approx 0.3$ for a hydrogen/helium mixture. We used a subset of data from 0.5 bars to 18 bars (MSY stated very low confidence in measurements deeper than 18 bars). The heat capacity is therefore considered constant, which is an adequate approximation for the limited range of temperatures and pressures measured by the GP (MSY). The lapse rate was interpolated in the vertical to a constant pressure interval of 0.2 bar.

Figure 1 (left column) includes a guess about the orientation of θ and *M* surfaces in the neighborhood of the GP sounding, assuming to leading order that the flow is geostrophic and therefore zonal thermal wind balance holds (a steady state relation between vertical geostrophic wind shear, which is observed, and horizontal temperature gradients). Figure 1 (right column) shows orientations of $\nabla \theta$ and ∇M for the high-shear region at 2 bars (A), and the low-shear region at 14 bars (B), using observed values from the GP and the Cassini mission [*Porco et al.*, 2003], and deep thermal wind balance. Errors were retrieved from MSY for $\partial \theta / \partial z$, *Atkinson et al.* [1997] for $\partial u / \partial z$, and *Porco et al.* [2003] for $\partial u / \partial y$. The error of the high-shear $\partial \theta / \partial y$, calculated via the deep thermal wind relation, was estimated to be approximately 15%. The corresponding error of the low-shear region $\partial \theta / \partial y$ calculation was estimated to be approximately 30%, due to the larger slope in that region and some uncertainty in the exact corresponding depth of the interpolated lapse rate. It is likely that compounded errors are still underestimated; for example, we assume that contributions to $\partial \theta / \partial y$ due to diabatic forcing/insolation are 0. The present assessment suggests that PV could plausibly equal 0 in the high-shear region, because $\nabla \theta$ and ∇M gradients are virtually antiparallel.

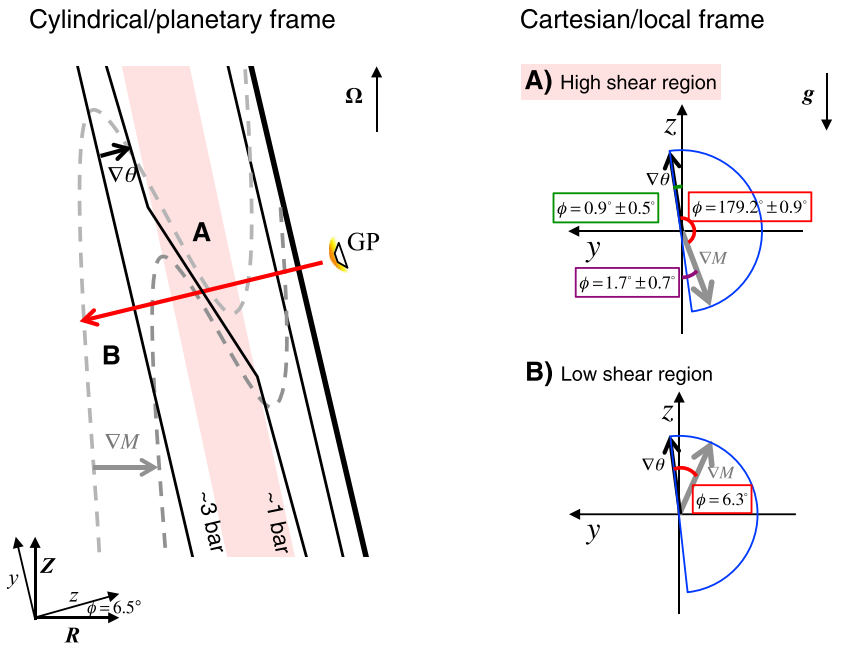

Figure 1. Schematics of the Galileo probe path relative to θ and M surfaces. (left column) The GP entry path for a cylindrical coordinate system, such that "up" is parallel to the spin axis. It shows the high-shear region in which both M and θ surfaces are tilted and in fact antiparallel, such that the fluid is essentially adiabatic in spite of an observed stable lapse rate in the vertical. The Galileo probe path (red arrow) crossed M surfaces that appear to fold over in the high-shear region, where the figure shows a proposed M field that would satisfy observations. (right column) SI semicircle diagrams adapted from *Fruman and Shepherd* [2008], using the GP winds and MSY static stability. The diagrams are in a local Cartesian frame at 6.5°N with gravity pointing downward. In both cases, the semicircle that indicates symmetric stability (equivalently, PV$\propto \nabla\theta \times \nabla M > 0$) is shown in blue, such that if ∇M lies outside this circle, PV<0. In both cases $\partial\theta/\partial y$ has been estimated using deep thermal wind balance with the observed wind shear at each depth. Small angles are exaggerated for demonstration purposes.

4. Measuring Lapse Rates Amidst Slantwise Convection

Zero PV is consistent with a fluid that has been neutralized to SI, implying that the observed static stability is not in fact dynamically relevant in this region. Instead, the fluid here is possibly adiabatic, and the static stability may be assessed more appropriately along constant M surfaces. We shall refer to a lapse rate taken at constant M as Γ_M to distinguish it from the observed GP vertical lapse rate Γ_z and proceed to calculate Γ_M from the observations assuming geostrophic and deep thermal wind balance [*Kaspi et al.*, 2009]. Such a calculation should yield $\Gamma_M = 0$ in regions where the Richardson number is less than or equal to 1, indicating SI, and yield meaningless, nonzero Γ_M where SI is not playing a significant role in the dynamics.

Though the GP sounding undoubtedly involves a complicated local flow [*Showman and Ingersoll*, 1998; *Showman and Dowling*, 2000], a fully 3-D development is beyond the scope of this paper, and we focus on assuming zonal geostrophic balance. This method can work broadly for understanding the lapse rate of any zonally elongated structure in $Ri \approx 1$ flow and may be of utility for the GP observations as well if the flow is sufficiently zonally elongated.

Emanuel [1985] provided an equation for Γ_M that is suitable for the midlatitudes of shallow terrestrial atmospheres, by accounting for the tilting of potential temperature surfaces due to thermal wind balance. We generalize the relation to deep, zonal atmospheric flow at any latitude by employing geostrophic coordinates, commonly used in studies of midlatitude frontogenesis [*Hoskins and Bretherton*, 1972; *Hoskins*, 1975].

To assess the appropriate along-momentum surface lapse rate, we define a pseudomomentum M, which is a linearized proxy for absolute angular momentum per unit mass [*Emanuel*, 1983a]. Let M in local Cartesian coordinates be $M = u_g - (2\Omega \sin\phi)y + (2\Omega \cos\phi)z$, for northward $+y$, upward (radial) $+z$, geostrophic wind u_g, and planetary rotation frequency Ω. In a deep atmosphere, thermal wind balance is $g/\theta_0(\partial\theta/\partial y) = -[2\Omega \cos(\phi)\partial M/\partial y + 2\Omega \sin(\phi)\partial M/\partial z]$, which includes an additional term to account for the horizontal component of the Coriolis force.

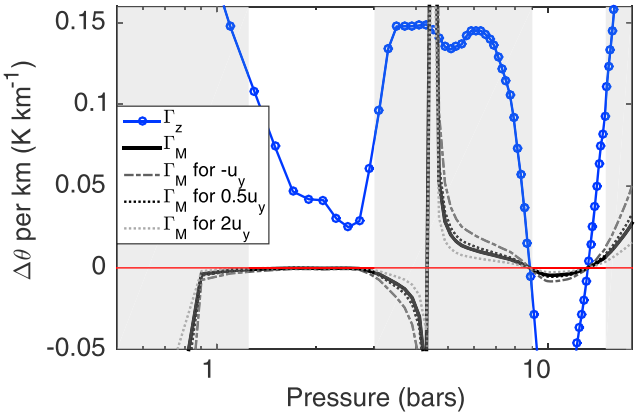

Figure 2. The observed and angular momentum-adjusted *Galileo* lapse rates. Γ_z (blue line) as reported by MSY, and Γ_M, showing the significantly smaller equivalent lapse rate on M surfaces. Regions where MSY estimate that Ri is around 0.25 are indicated by the white background, and these are the regions for which the adjusted lapse rate Γ_M is applicable. The shear $\partial u/\partial y \equiv u_y$ used to calculate Γ_M is taken from the Cassini mean wind profile [*Porco et al.*, 2003] at the latitude of the GP entry, and while strongly positive, it is still over 3 orders of magnitude smaller than $\partial u_g/\partial z$. Other possibilities for meridional wind shear are provided by the dashed lines for illustration of sensitivity to meridional shear. The red line indicates a lapse rate of 0, and the x axis is a log scale.

While soundings are taken in the local vertical z, a more applicable coordinate system for M on a rotating planet is cylindrical, such that R is the distance from the spin axis and Z is the distance from the equatorial plane. In solid body rotation, $\partial M/\partial R = 2\Omega$, and $\partial M/\partial Z = 0$. However, because wind shear can tilt M surfaces, we ultimately desire a geostrophic coordinate system (R^*, Z^*) that follows M surfaces for any zonal, geostrophically balanced wind. In such a coordinate system, the gradient operator $\partial/\partial Z^*$ can evaluate dynamically relevant lapse rates along M surfaces: $\partial\theta/\partial Z^* = \Gamma_M$.

After the transformation into geostrophic coordinates (see Appendix), the expression for Γ_M is

$$\Gamma_M = \cos\phi\frac{\partial\theta}{\partial y} + \sin\phi\frac{\partial\theta}{\partial z} + \frac{g}{2\Omega\xi\theta_0}\frac{\partial\theta}{\partial y}\left(\cos\phi\frac{\partial\theta}{\partial z} - \sin\phi\frac{\partial\theta}{\partial y}\right) \quad (1)$$

for absolute vorticity ξ parallel to the spin axis, reference temperature $\theta_0 = 165$ K at 1 bar and gravity profile $g(z)$ as estimated by the GP analysis. Solving for Γ_M requires three main assumptions: the measured wind is zonal, the flow is to leading order geostrophic and therefore in thermal wind balance, and the meridional shear of the zonal geostrophic wind $\partial u/\partial y$ is approximated by the observed Cassini wind profile [*Porco et al.*, 2003]. An additional simplifying assumption is that solar insolation does not induce radiatively driven $\partial\theta/\partial y$, which is unlikely in the upper troposphere but a better assumption below 1 bar, the level at which most solar radiation is absorbed [*Sanchez-Lavega et al.*, 2008].

The calculation of equation (1) is provided by Figure 2, including the observed vertical shear $\partial u/\partial z$ and estimated meridional shear $\partial u/\partial y$. The main result is that where MSY claimed that $Ri = 0.25$ (white regions), Γ_M is indeed virtually 0. This is particularly clear in the $1.25 < p < 3$ bar region and supports the hypothesis that this layer in the atmosphere is actually adiabatic, in spite of the observed vertical static stability. The meridional shear estimate $\partial u/\partial y$ was only measured at cloud top in the zonal mean [*Porco et al.*, 2003], and there is a lot of uncertainty about the in situ horizontal wind shear because of the unique hot spot morphology [*Showman and Dowling*, 2000] and lack of cloud tracers. Figure 2 shows the solution of equation (1) for several other horizontal shears, to illustrate robustness of the results to a range of horizontal wind shears.

The dramatic, nearly vertical slopes of Γ_M in Figure 2 are due to the change in sign of $\partial M/\partial z$, both above and below the adiabatic layer in which the M surfaces fold over. In these transition areas Ri is likely to be above 1 (MSY), so the adjusted lapse rate Γ_M is not applicable.

5. Possibility of Observing Tilted Convective Features

A direct implication of this adiabatic layer and consequent slantwise convection is that meteorological features in Jupiter's equatorial region may exhibit small meridional tilts with altitude. Detection of

such vertical misalignments in a rapidly evolving atmosphere presents a considerable challenge without near-simultaneous remote sensing across a broad range of wavelengths. For example, the *Juno* mission's microwave [*Janssen et al.*, 2005] observations and Earth-based radio wave [*de Pater et al.*, 2016] observations sounding ammonia and temperature contrasts deep below the visible clouds (1–100 bars) must be concurrent with thermal infrared observations sounding upper tropospheric temperature and composition (0.1–0.7 bar [e.g., *Fletcher et al.*, 2016]), 5 μm observations sensing gaps in 2–4 bar cloud opacity [e.g., *Ortiz et al.*, 1998], and reflected-sunlight observations in the visible and near-IR probing aerosol structure in the 0.1–1.0 bar region [e.g., *Porco et al.*, 2003]. This simultaneity across multiple wavelengths and facilities may allow us for the first time to resolve the expected along-*M* tilt of elongated features on a global scale.

Identification of slantwise convection using existing visible and infrared data is challenging. Imaging across such a broad wavelength range is rarely simultaneous, such that spatial misalignments of convective features from observation to observation could simply be explained by Jupiter's temporally variable atmosphere. Furthermore, the spatial resolution of observations in different wave bands must be similar, in order to probe the small scales described here.

Two recent observations do hint at tilted meteorological structures. First, ammonia-rich plumes immediately south of Jupiter's prograde equatorial jet at 6.8°N are thought to be the rising branch of the wave pattern, which then descends within the hot spots that are slightly farther north [*Allison*, 1990; *Showman and Dowling*, 2000; *Baines et al.*, 2002]. However, this meridional offset could simply be a natural consequence of the wave pattern (typically interpreted as an equatorially trapped Rossby wave) that forms the hot spots [*Friedson*, 2005]. Second, the Great Red Spot is known to be asymmetric in the latitudinal direction, with higher 500 mbar temperatures, depleted NH_3 gas, and deeper cloud tops toward the southern edge of the vortex [*Simon-Miller et al.*, 2002; *Fletcher et al.*, 2010], suggesting that the Great Red Spot has a "tilted pancake" or "wedge-shaped" structure [*Simon-Miller et al.*, 2002]. This may be more closely related to the dynamics of the vortex over large spatial scales than to slantwise convection. On smaller scales, isolated moist-convective systems (tens to hundreds of kilometers across) are not expected to exhibit the slantwise convective tilt because they lack the required zonal elongation that approximately conserves *M*. However, any observational improvements that better resolve deep convection may also betray equatorial zonal mean tilts, for example in the belt/zone structure [e.g., *Sanchez-Lavega et al.*, 1996].

6. Conclusion

Existing theoretical, numerical, and observational literature shows that SI can occur in 3-D nonlinear fluids, in regions of limited extent, in the presence of competing instabilities. The resulting slantwise bands of convection that mix the fluid with nearby high PV air to drive it to PV = 0 can be tilted horizontally [*Jones and Thorpe*, 1992] as well as vertically [*Bennetts and Hoskins*, 1979], and in frontal zones the 3-D signature of SI can dominate for long time periods [*Arobone and Sarkar*, 2015]. Jupiter exhibits numerous, filamented bands of convection in the equatorial region and provides an excellent laboratory for potential observation of slantwise convection. The GP itself offers sufficient clues to suggest that SI has already been observed.

The proposed adiabatic layer at $1.25 < p < 3$ bars is 35 km thick, approximately a scale height. The present analysis relies on a wave analysis of MSY, where $Ri = 0.25$ was chosen as a convective threshold. However, the wave analysis was not sensitive to the range of *Ri* between 0.25 and 1, and this is where SI and slantwise convection can induce zero lapse rates. Using a coordinate system that moves with the geostrophic wind, we find that the high-shear region in particular suggests that SI is occurring: first, PV = 0 within the error of the instruments, and second, a lapse rate calculated for observed and balanced quantities shows that Γ_M is 0 as well. Thus, a thick atmospheric layer that is approximately neutral to convection sits in the midtroposphere in the region of the GP, in spite of the positive static stability measured in the vertical. This is consistent with the residual wind speeds observed by the GP and examined by *Allison and Atkinson* [2001]. Perhaps what has been interpreted as a wave signature is actually the overturning circulation due to slantwise convecting cells adjusting the low *Ri* layer back to PV = 0.

A dry potential temperature is used here instead of a virtual potential temperature, which would account for water loading, because the GP measured a remarkably dry, subsolar concentration of oxygen (and, consequently, water) [*Niemann et al.*, 1998]. This was fortunate because it is simpler to calculate. Water loading effects will be very complicated and are a rich area of exploration [see *Fantini and Malguzzi*, 2008]. Ultimately,

SI occurs because of diabatic forcing that locally changes the sign of PV, and it is difficult to motivate this without latent heat release. There should be ample latent heating on Jupiter; indeed, there are regular lightning storms [*Little et al.*, 1999]. Why did the GP observe an adiabatic layer? Are the hot spots preferentially cooling to space, at a rate that can drive down the static stability of the 1–3 bar region sufficiently? Another complicating consideration is the stabilizing property of the radial molecular gradient [e.g., *Li and Ingersoll*, 2015; *Leconte et al.*, 2016]. For this study that can be safely neglected, because MSY found that the GP observations of the molecular gradients were small enough to not affect their analysis. Globally, both water and molecular gradients will need to be taken into account when determining where the fluid is actually adiabatic.

Possibility of SI and slantwise convection presented here may be broadly applicable, depending on the *Ri* measured by NASA's ongoing *Juno* observations (2016–2019). Conclusive evidence of slanted convection and vertical misalignments in Jupiter's low latitudes must await simultaneous observations from multiple facilities across a wide wavelength range. Deep-seated convective features observed at ≈1000 km length scales may be observed by *Juno*'s microwave radiometer [*Janssen et al.*, 2005] and can be compared to visible, infrared, and radio wave imaging from Earth.

Appendix A: Geostrophic Coordinates

Assume that all flow is axisymmetric about the spin axis. In solid body rotation (SBR), absolute angular momentum M should vary strictly in R, for a cylindrical coordinate system with distance from the equatorial plane Z and distance from the spin axis R. Also, in SBR (neglecting solar insolation), temperature should vary only in the local vertical direction z. Because these variations take place in coordinate systems rotated relative to one another around the planet's center of mass, their relation is a function of latitude ϕ.

$$\frac{\partial}{\partial R} = -\sin\phi\frac{\partial}{\partial y} + \cos\phi\frac{\partial}{\partial z} \tag{A1}$$

$$\frac{\partial}{\partial Z} = \cos\phi\frac{\partial}{\partial y} + \sin\phi\frac{\partial}{\partial z}. \tag{A2}$$

As in section 4, let the linearized pseudomomentum M in local Cartesian coordinates be $M = u_g - (2\Omega\sin\phi)y + (2\Omega\cos\phi)z$, for northward $+y$, upward (radial) $+z$, geostrophic wind u_g, and planetary rotation frequency Ω. We desire a coordinate system that is everywhere aligned with M, such that even in the presence of wind shear, M varies only in one direction, R^*. Let our new geostrophic coordinates be (R^*, Z^*) [*Hoskins and Bretherton*, 1972; *Hoskins*, 1975]. Define R^* such that $M = 2\Omega R^*$. Thus, $R^* = R + u_g/(2\Omega)$ and $Z^* = Z$. In zonal geostrophic balance, $\partial M/\partial Z^* = 0$.

The Jacobian for the coordinate transformation is $\partial(R^*, Z^*)/\partial(R, Z)$.

$$J = \begin{vmatrix} \frac{\partial R^*}{\partial R} & \frac{\partial R^*}{\partial Z} \\ \frac{\partial Z^*}{\partial R} & \frac{\partial Z^*}{\partial Z} \end{vmatrix} = \begin{vmatrix} \left(1 + \frac{1}{2\Omega}\frac{\partial u_g}{\partial R}\right) & \left(\frac{1}{2\Omega}\frac{\partial u_g}{\partial Z}\right) \\ 0 & 1 \end{vmatrix} \tag{A3}$$

$$= \left(1 + \frac{1}{2\Omega}\frac{\partial u_g}{\partial R}\right) \tag{A4}$$

$$= \xi/(2\Omega), \tag{A5}$$

for absolute vorticity ξ parallel to the spin axis. Transform the derivatives of $M = 2\Omega R^*$:

$$\frac{\partial M}{\partial R} = \frac{\xi}{2\Omega}\frac{\partial M}{\partial R^*} = \xi \tag{A6}$$

$$\Rightarrow \frac{\partial M}{\partial R^*} = 2\Omega \tag{A7}$$

$$\frac{\partial M}{\partial Z} = \left(\frac{1}{2\Omega}\frac{\partial u_g}{\partial Z}\right)\frac{\partial M}{\partial R^*} + \frac{\partial M}{\partial Z^*} \tag{A8}$$

$$= \frac{\partial u_g}{\partial Z} \tag{A9}$$

$$\Rightarrow \frac{\partial M}{\partial Z^*} = 0. \tag{A10}$$

Apply the gradient operators to the potential temperature θ:

$$\frac{\partial\theta}{\partial R} = \frac{\xi}{2\Omega}\frac{\partial\theta}{\partial R^*} \tag{A11}$$

$$\frac{\partial\theta}{\partial Z} = \left(\frac{1}{2\Omega}\frac{\partial u_g}{\partial Z}\right)\frac{\partial\theta}{\partial R^*} + \frac{\partial\theta}{\partial Z^*}. \tag{A12}$$

This last equation can be rearranged to make an expression for a lapse rate on constant M surfaces, $\Gamma_M = \partial\theta/\partial Z^*$. However, the observed lapse rate is measured in local Cartesian z and this expression is in cylindrical coordinates, so we use the following substitution (recall that $\partial u_g/\partial z = \partial M/\partial z$):

$$\frac{\partial M}{\partial Z} = \cos\phi\frac{\partial M}{\partial y} + \sin\phi\frac{\partial M}{\partial z}. \tag{A13}$$

The horizontal temperature gradient $\partial\theta/\partial y$ is unknown and can be replaced by the deep thermal wind equation,

$$2\Omega\cos\phi\frac{\partial M}{\partial y} + 2\Omega\sin\phi\frac{\partial M}{\partial z} = -\frac{g}{\theta_0}\frac{\partial\theta}{\partial y}. \tag{A14}$$

Keeping the unknown $\partial\theta/\partial y$ in equation (A12) for brevity, we arrive at an expression for Γ_M in Cartesian coordinates (1):

$$\Gamma_M = \cos\phi\frac{\partial\theta}{\partial y} + \sin\phi\frac{\partial\theta}{\partial z} + \frac{g}{2\Omega\xi\theta_0}\frac{\partial\theta}{\partial y}\left(\cos\phi\frac{\partial\theta}{\partial z} - \sin\phi\frac{\partial\theta}{\partial y}\right). \tag{A15}$$

If there is no wind shear, in which case the planet is in solid body rotation and $\partial M/\partial Z = 0$, then $\partial\theta/\partial y = 0$ and the thermal wind substitution equals 0. The only remaining equality is $\partial\theta/\partial Z^* = \sin\phi\partial\theta/\partial z$. This states that the local vertical lapse rate has a component along the spin axes proportional to $\sin\phi$ such that an arbitrarily large $\partial\theta/\partial z$ at the equator will have no impact on the zero-PV state, $\partial\theta/\partial Z^*$ (which in SBR equals $\partial\theta/\partial Z$).

This expression collapses to narrower cases in previous literature:

A1. At the Equator

At the equator, the absolute vorticity $\partial M/\partial R = \xi = 2\Omega + \partial u/\partial z$ and $\partial M/\partial Z = \partial u/\partial y$.

$$\frac{\partial\theta}{\partial Z^*} = -\left(\frac{2\Omega\theta_0}{g} + \frac{1}{\xi}\frac{\partial\theta}{\partial z}\right)\left(\frac{\partial u}{\partial y}\right). \tag{A16}$$

In the absence of horizontal shear, there is no temperature gradient along M surfaces. If $\partial u/\partial y$ is positive, $\partial\theta/\partial Z^* < 0$ and the fluid is symmetrically unstable [*Dunkerton*, 1981]. Observations of equatorial winds on both Jupiter and Saturn show that there is a local minimum in prograde winds right at the equator, with prograde jets increasing to a local maximum several degrees off the equator. However, this likely does not lead to symmetric instability because the decrease in the planetary component M when one moves poleward is sufficient to counteract the increase in M due to increasing winds.

A2. At the Pole

Note that $\xi = \partial M/\partial R$, which at the pole equals $-\partial M/\partial y$, and $\partial M/\partial Z$ at the pole is simply $\partial M/\partial z$:

$$\frac{\partial\theta}{\partial Z^*} = \frac{\partial\theta}{\partial z} - \left(\frac{\partial M/\partial z}{\partial M/\partial y}\right)\frac{\partial\theta}{\partial y}. \tag{A17}$$

This is equivalent to equation (15) of *Emanuel* [1985]. If the fluid is adiabatic (PV = 0), $\partial\theta/\partial Z^* = 0$ and the tilt of M and θ surfaces is identical:

$$\frac{\partial\theta/\partial z}{\partial\theta/\partial y} = \frac{\partial M/\partial z}{\partial M/\partial y}. \tag{A18}$$

Acknowledgments
The authors appreciate helpful conversations with Andy Ingersoll, Michael Allison, Sushil Atreya, Glenn Flierl, and Kerry Emanuel. M.O'N. and Y.K. gratefully acknowledge support from the Israeli Ministry of Science, the Minerva Foundation, and the Weizmann Institute of Science (WIS) Helen C. Kimmel Center for Planetary Science. M.O'N. was also supported by the WIS Koshland Postdoctoral Fellowship. L.N.F. was supported by a Royal Society Research Fellowship at the University of Leicester. Wind, pressure, gravity, and altitude data from NASA's Galileo Probe Doppler Wind Experiment were retrieved from http://pds-atmospheres.nmsu.edu/PDS/data/gp_0001/data/dwe, from the Atmospheric Structure Instrument (http://pds-atmospheres.nmsu.edu/PDS/data/gp_0001/data/dwe/asi4atm.lbl), and other data used are available from the references below.

References

Allison, M. (1990), Planetary waves in Jupiter's equatorial atmosphere, *Icarus*, *83*(2), 282–307.
Allison, M., and D. Atkinson (2001), Galileo probe Doppler residuals as the wave-dynamical signature of weakly stable, downward-increasing stratification in Jupiter's deep wind layer, *Geophys. Res. Lett.*, *28*(14), 2747–2750.

Allison, M., A. D. Del Genio, and W. Zhou (1995), Richardson number constraints for the Jupiter and outer planet wind regime, *Geophys. Res. Lett.*, *22*(21), 2957–2960.
Arobone, E., and S. Sarkar (2015), Effects of three-dimensionality on instability and turbulence in a frontal zone, *J. Fluid Mech.*, *784*, 252–273.
Atkinson, D. H., A. P. Ingersoll, and A. Seiff (1997), Deep winds on Jupiter as measured by the Galileo probe, *Nature*, *388*(6643), 649–650.
Baines, K. H., R. W. Carlson, and L. W. Kamp (2002), Fresh ammonia ice clouds on Jupiter: I. Spectroscopic identification, spatial distribution, and dynamical implications, *Icarus*, *159*(1), 74–94.
Bennetts, D. A., and B. J. Hoskins (1979), Conditional symmetric instability—A possible explanation for frontal rainbands, *Q. J. R. Meteorol. Soc.*, *105*(446), 945–962.
Charney, J. G. (1973), *Dynamic Meteorology: Lectures Delivered at the Summer School of Space Physics of the Centre National D'Etudes Spatiales, Held at Lannion, France, 7 August–12 September 1970*, chap. Planetary Fluid Dynamics, pp. 97–351, Springer, Dordrecht, Netherlands.
D'Asaro, E., C. Lee, L. Rainville, R. Harcourt, and L. Thomas (2011), Enhanced turbulence and energy dissipation at ocean fronts, *Science*, *332*(6027), 318–322.
de Pater, I., R. J. Sault, B. Butler, D. DeBoer, and M. H. Wong (2016), Peering through Jupiter's clouds with radio spectral imaging, *Science*, *352*(6290), 1198–1201.
deVerdiere, A. C. (2012), The stability of short symmetric internal waves on sloping fronts: Beyond the traditional approximation, *J. Phys. Ocean.*, *42*(3), 459–475.
Dunkerton, T. J. (1981), On the inertial stability of the equatorial middle atmosphere, *J. Atmos. Sci.*, *38*(11), 2354–2364.
Dunkerton, T. J. (1983), A nonsymmetric equatorial inertial instability, *J. Atmos. Sci.*, *40*(3), 807–813.
Eady, E. T. (1949), Long waves and cyclone waves, *Tellus*, *1*, 33–52.
Emanuel, K. A. (1979), Inertial instability and mesoscale convective systems. Part I: Linear theory of inertial instability in rotating viscous fluids, *J. Atmos. Sci.*, *36*(12), 2425–2449.
Emanuel, K. A. (1983a), The Lagrangian parcel dynamics of moist symmetric instability, *J. Atmos. Sci.*, *40*(10), 2368–2376.
Emanuel, K. A. (1983b), On assessing local conditional symmetric instability from atmospheric soundings, *Mon. Weather Rev.*, *111*(10), 2016–2033.
Emanuel, K. A. (1985), Convective adjustment in baroclinic atmospheres, in *The Jovian Atmospheres*, vol. 2441 in Conference Proceedings, edited by M. Allison and and L. D. Travis, pp. 163–171, NASA, NASA Scientific and Technical Information Branch, New York.
Fantini, M., and P. Malguzzi (2008), The slope of moist symmetric instability with water loading, *J. Atmos. Sci.*, *65*(9), 2922–2935.
Flasar, F. M., and P. J. Gierasch (1986), Mesoscale waves as probe of Jupiter's deep atmosphere, *J. Atmos. Sci.*, *43*, 2683–2707.
Fletcher, L. N., et al. (2010), Thermal structure and composition of Jupiter's Great Red Spot from high-resolution thermal imaging, *Icarus*, *208*(1), 306–328.
Fletcher, L. N., T. K. Greathouse, G. S. Orton, J. A. Sinclair, R. S. Giles, P. G. J. Irwin, and T. Encrenaz (2016), Mid-infrared mapping of Jupiter's temperatures, aerosol opacity and chemical distributions with IRTF/TEXES, *Icarus*, *278*, 128–161.
Friedson, A. J. (2005), Water, ammonia, and H_2S mixing ratios in Jupiter's five-micron hot spots: A dynamical model, *Icarus*, *177*, 1–17.
Fruman, M. D., and T. G. Shepherd (2008), Symmetric stability of compressible zonal flows on a generalized equatorial-plane, *J. Atmos. Sci.*, *65*(6), 1927–1940.
Guillot, T., D. J. Stevenson, W. B. Hubbard, and D. Saumon (2004), The interior of Jupiter, in *Jupiter: The Planet, Satellites and Magnetosphere*, edited by F. Bagenal, T. E. Dowling, and W. B. McKinnon, pp. 35–57, Cambridge Univ. Press, Cambridge, U. K.
Haine, T. W. N., and J. Marshall (1998), Gravitational, symmetric, and baroclinic instability of the ocean mixed layer, *J. Phys. Oceanogr.*, *28*(4), 634–658.
Hoskins, B. J. (1974), The role of potential vorticity in symmetric stability and instability, *Q. J. R. Meteorol. Soc.*, *100*(425), 480–482.
Hoskins, B. J. (1975), The geostrophic momentum approximation and the semi-geostrophic equations, *J. Atmos. Sci.*, *32*(2), 233–242.
Hoskins, B. J., and F. P. Bretherton (1972), Atmospheric frontogenesis models: Mathematical formulation and solution, *J. Atmos. Sci.*, *29*(1), 11–37.
Hubbard, W. B. (1977), The Jovian surface condition and cooling rate, *Icarus*, *30*(2), 305–310.
Ingersoll, A. P. (1990), Atmospheric dynamics of the outer planets, *Science*, *248*(4953), 308–315.
Itano, T., and K. Maruyama (2009), Symmetric stability of zonal flow under full-component Coriolis force—Effect of the horizontal component of the planetary vorticity, *J. Meteo. Soc. Jpn. Ser. II*, *87*(4), 747–753.
Janssen, M. A., M. D. Hofstadter, S. Gulkis, A. P. Ingersoll, M. Allison, S. J. Bolton, S. M. Levin, and L. W. Camp (2005), Microwave remote sensing of Jupiter's atmosphere from an orbiting spacecraft, *Icarus*, *173*(2), 447–453.
Jeffery, N., and B. Wingate (2009), The effect of tilted rotation on shear instabilities at low stratifications, *J. Phys. Oceanogr.*, *39*(12), 3147–3161.
Jones, S. C., and A. J. Thorpe (1992), The three-dimensional nature of 'symmetric' instability, *Q. J. R. Meteorol. Soc.*, *118*(504), 227–258.
Kaspi, Y., G. R. Flierl, and A. P. Showman (2009), The deep wind structure of the giant planets: Results from an anelastic general circulation model, *Icarus*, *202*(2), 525–542.
Leconte, J., F. Selsis, F. Hersant, and T. Guillot (2016), Condensation-inhibited convection in hydrogen-rich atmospheres: Stability against double-diffusive processes and thermal profiles of Jupiter, Saturn, Uranus, and Neptune, *Astron. Astrophys.*, *598*, A98.
Li, C., and A. P. Ingersoll (2015), Moist convection in hydrogen atmospheres and the frequency of Saturn's giant storms, *Nat. Geosci.*, *8*(5), 398–403.
Little, B., D. A. Clifford, A. P. Ingersoll, A. R. Vasavada, D. A. Senske, H. H. Breneman, W. J. Borucki, and the Galileo SSI Team (1999), Galileo images of lightning on Jupiter, *Icarus*, *142*(2), 306–323.
Magalhães, J. A., A. Seiff, and R. E. Young (2002), The stratification of Jupiter's troposphere at the Galileo probe entry site, *Icarus*, *158*(2), 410–433.
Niemann, H. B., S. K. Atreya, G. R. Carignan, T. M. Donahue, J. A. Haberman, D. N Harpold, R. E. Hartle, D. M. Hunten, W. T. Kasprzak, P. R. Mahaffy, T. C. Owen, and S. H. Way (1998), The composition of the Jovian atmosphere as determined by the Galileo probe mass spectrometer, *J. Geophys. Res.*, *103*(E10), 22,831–22,845.
O'Neill, M. E, and Y. Kaspi (2016), Slantwise convection on fluid planets, *Geophys. Res. Lett.*, *43*(20), 10,611–10,620.
Ooyama, K. (1966), On the stability of the baroclinic circular vortex: A sufficient criterion for instability, *J. Atmos. Sci.*, *23*(1), 43–53.
Ortiz, J. L., G. S. Orton, A. J. Friedson, S. T. Stewart, B. M. Fisher, and J. R. Spencer (1998), Evolution and persistence of 5-μm hot spots at the Galileo probe entry latitude, *J. Geophys. Res.*, *103*(E10), 23,051–23,069.
Orton, G. S., et al. (1998), Characteristics of the Galileo probe entry site from Earth-based remote sensing observations, *J. Geophys. Res.*, *103*(E10), 22,791–22,814.
Porco, C. C., et al. (2003), Cassini imaging of Jupiter's atmosphere, satellites and rings, *Science*, *299*(5612), 1541–1547.

Sanchez-Lavega, A., J. M. Gomez, J. Lecacheux, F. Coles, I. Miyazaki, D. Parker, and J. Guarro (1996), The South Equatorial Belt of Jupiter, II: The onset and development of the 1993 disturbance, *Icarus*, *121*(1), 18–29.
Sanchez-Lavega, A., et al. (2008), Depth of a strong Jovian jet from a planetary-scale disturbance driven by storms, *Nature*, *451*(7177), 437–440.
Sanders, F. (1986), Frontogenesis and symmetric stability in a major New England snowstorm, *Mon. Weather Rev.*, *114*, 1847–1862.
Seiff, A., D. B. Kirk, T. C. D. Knight, R. E. Young, J. D. Mihalov, L. A. Young, F. S. Milos, G. Schubert, R. C. Blanchard, and D. Atkinson (1998), Thermal structure of Jupiter's atmosphere near the edge of a 5-μm hot spot in the North Equatorial Belt, *J. Geophys. Res.*, *103*(E10), 22,857–22,889.
Showman, A. P., and T. E. Dowling (2000), Nonlinear simulations of Jupiter's 5-micron hot spots, *Science*, *289*(5485), 1737–1740.
Showman, A. P., and A. P. Ingersoll (1998), Interpretation of Galileo probe data and implications for Jupiter's dry downdrafts, *Icarus*, *132*(2), 205–220.
Simon-Miller, A. A., P. J. Gierasch, R. F. Beebec, B. Conrath, F. M. Flasar, R. K. Achterberg, and the Cassini CIRS Team (2002), New observational results concerning Jupiter's Great Red Spot, *Icarus*, *158*(1), 249–266.
Stamper, M. A., and J. R. Taylor (2017), The transition from symmetric to baroclinic instability in the Eandy model, *Ocean Dyn.*, *67*(1), 65–80.
Stone, P. H. (1966), On non-geostrophic baroclinic stability, *J. Atmos. Sci.*, *23*(4), 390–400.
Stone, P. (1967), An application of baroclinic stability theory to the dynamics of the Jovian atmosphere, *J. Atmos. Sci.*, *24*, 642–652.
Stone, P. (1970), On non-geostrophic baroclinic stability: Part II, *J. Atmos. Sci.*, *27*(5), 721–726.
Straneo, F., M. Kawase, and S. C. Riser (2002), Idealized models of slantwise convection in a baroclinic flow, *J. Phys. Oceanogr.*, *32*(2), 558–572.
Taylor, J. R., and R. Ferrari (2009), On the equilibration of a symmetrically unstable front via a secondary shear instability, *J. Fluid Mech.*, *622*, 103–113.
Thomas, L. N., J. R. Taylor, R. Ferrari, and T. M. Joyce (2013), Symmetric instability in the Gulf Stream, *J. Phys. Oceanogr.*, *46*, 197–217.
Thomas, L. N., J. R. Taylor, E. A. D'Asaro, C. M. Lee, J. M. Klymak, and A. Shcherbina (2016), Symmetric instability, inertial oscillations, and turbulence at the Gulf Stream front, *J. Phys. Oceanogr.*, *46*, 197–217.
Thorpe, A. S., and R. Rotunno (1989), Nonlinear aspects of symmetric instability, *J. Atmos. Sci.*, *46*(9), 1285–1299.
Young, R. E. (1998), The Galileo probe mission to Jupiter: Science overview, *J. Geophys. Res.*, *103*(E10), 22775–22790.